Elasto/Visco-Plastic Deformation of Shells of Revolution under Thermal Loading due to Fluid*

Shigeo TAKEZONO**, Katsumi TAO**,
Takashi AOKI*** and Eijiroh INAMURA**

An analytical method for the elasto/visco-plastic deformation of axisymmetrical thin shells subjected to thermal loads due to fluid is developed. First, the temperature distribution through the thickness is assumed to be a curve of the second order, and the temperature field in the shell under appropriate initial and boundary conditions is determined using the equations of heat conduction and heat transfer. Secondly, the stresses and deformations are derived from the thermal stress equations. The equations of equilibrium and the relationships between the strains and displacements are derived from the Sanders elastic shell theory. For the constitutive relations, the Perzyna elasto/visco-plastic equations which consider the temperature effect are employed. The fundamental equations derived are numerically solved using the finite difference method. As a numerical example, a simply supported internally pressurized cylindrical shell of aluminum under thermal loading due to fluid is analyzed, and the variations in displacements and internal forces with time are discussed.

Key Words: Structural Analysis, Theory of Shell, Thermal Stress, Finite Difference Method, Elasto/Visco-Plasticity, Heat Conduction

1. Introduction

For elasto/visco-plastic deformation of shells, many investigations have been carried out, not only for axisymmetrical shells, but also for general asymmetrical shells. These investigations, however, deal with cases where a constant temperature distribution is maintained in the shell body[1)-7)]. Only a few investigations of problems concerned with nonuniform temperature distribution have been performed[8),9)].

In the present paper the authors develop an analytical method for thermo-elasto/visco-plastic deformation of axisymmetrical thin shells of revolution. Regarding the heat conduction of shells, up to now, almost all investigators have assumed the temperature distribution through the thickness to be linear[10)-12)], but we suppose it to be a curve of the second order, considering the heat transfer on the shell surface. First, the temperature field in the shell under appropriate initial and boundary conditions is determined using the equations of heat conduction and heat transfer. Secondly, the stresses and deformations are derived from the thermal stress equations. The equations of equilibrium derived from the Sanders theory for thin shells[13)] are used. As the constitutive relations, Hooke's law is used in the elastic range, and the Perzyna elasto/visco-plastic equations[14)], including the temperature effect, are employed in the plastic range. The yield condition used in the analysis depends on von Mises yield theory. The fundamental equations derived are solved numerically by the finite difference method, and the solutions are obtained by integration of the incremental values.

As a numerical example, an internally pressurized cylindrical shell subjected to thermal load due to fluid is analyzed.

2. Fundamental Equations

If the middle surface of axisymmetrical shells is

* Received 14th February, 1994. Japanese original: Trans. Jpn. Soc. Mech. Eng., Vol. 59, No. 562, A (1993), p. 1443-1450 (Received 30th November, 1992)

** Department of Mechanical Engineering, Toyohashi University of Technology, Tempaku-cho, Toyohashi 441, Japan

*** Yaskawa Electric Mfg. Co., Ltd., Yahatanishi-ku, Kitakyushu 806, Japan

given by $r=r(s)$, where r is the distance from the axis and s is the meridional distance measured from a boundary along the middle surface as shown in Fig. 1, the relations among the nondimensional curvatures $\omega_\xi(=a/R_s)$, $\omega_\theta(=a/R_\theta)$ and the nondimensional radius $\rho(=r/a)$ become

$$\left.\begin{aligned}&\omega_\xi=-(\gamma'+\gamma^2)/\omega_\theta,\ \omega_\theta=\sqrt{1-(\rho')^2}/\rho\\&\omega'_\theta=\gamma(\omega_\xi-\omega_\theta),\ \rho''/\rho=-\omega_\xi\omega_\theta\\&\xi=s/a,\ \gamma=\rho'/\rho,\ (\ )'=d(\ )/d\xi\end{aligned}\right\}\quad(1)$$

where a is the reference length. An arbitrary point in the shell can be expressed in the orthogonal coordinate system (ξ, θ, ζ).

2.1 Heat conduction equations

The equation of heat conduction at a point in the shell body is given in the orthogonal coordinates (ξ, θ, ζ) as

$$\frac{\partial T}{\partial t}-\frac{\chi}{a^2}\left(\gamma\frac{\partial T}{\partial\xi}+\frac{\partial^2 T}{\partial\xi^2}+\frac{1}{\rho^2}\frac{\partial^2 T}{\partial\theta^2}\right)-\chi\frac{\partial^2 T}{\partial\zeta^2}-\frac{1}{c\rho_0}\eta_0=0\quad(2)$$

where T is the temperature at (ξ, θ, ζ, t), $\chi(=\lambda_0/c\rho_0)$ is the thermal diffusivity, c is the specific heat, ρ_0 is the mass density, λ_0 is the coefficient of thermal conductivity and η_0 is the heat generation per unit volume and per unit time.

The boundary conditions of the temperature on the inner and outer surfaces $(\zeta=\mp h/2)$ of the shell are

$$\left.\begin{aligned}&[\partial T/\partial\zeta]_{\zeta=-h/2}=h_i(T_{\text{in}}-\Theta_i)\\&[\partial T/\partial\zeta]_{\zeta=h/2}=-h_o(T_{\text{out}}-\Theta_o)\end{aligned}\right\}\quad(3)$$

where $h_i=k_i/\lambda_0$, $h_o=k_o/\lambda_0$ and k is the heat transfer coefficient. T_{in} and T_{out} are the temperatures on the inner and outer surfaces of the shell, Θ_i and Θ_o are ambient fluid temperatures of the shell, and h is the thickness of the shell.

The assumption that the temperature distribution through the thickness is linear, has been adopted by Bolotin[10], Shirakawa and Ochiai[11], Mizoguchi[12] and others. If this assumption is used, the boundary conditions of Eqs. (3) cannot be introduced in the derivation of Eqs. (5), and the resulting definite integral term becomes zero. In the present paper, to avoid the above difficulty and to improve the accuracy of the solutions for initial response stages, the temperature distribution through the thickness is assumed to be a curve of the second order by using coefficients T_0, T_1 and T_2 as follows:

$$T(\xi,\theta,\zeta,t)=T_0(\xi,\theta,t)+T_1(\xi,\theta,t)\zeta+T_2(\xi,\theta,t)\zeta^2.\quad(4)$$

After substituting Eq. (4) into Eq. (2), integrating Eq. (2), Eq. (2) multiplied by ζ, and Eq. (2) multiplied by ζ^2 through the thickness, with consideration of the surface boundary conditions (Eqs. (3)), we obtain the following three equations, respectively:

$$\left.\begin{aligned}&\frac{\partial}{\partial t}(T_0)+\frac{h^2}{12}\frac{\partial}{\partial t}(T_2)-\frac{\chi}{a^2}\Big[\gamma\frac{\partial}{\partial\xi}(T_0)+\frac{\partial^2}{\partial\xi^2}(T_0)+\frac{1}{\rho^2}\frac{\partial^2}{\partial\theta^2}(T_0)+\frac{h^2}{12}\Big\{\gamma\frac{\partial}{\partial\xi}(T_2)+\frac{\partial^2}{\partial\xi^2}(T_2)+\frac{1}{\rho^2}\frac{\partial^2}{\partial\theta^2}(T_2)\Big\}\Big]+\frac{\chi}{h}(h_o+h_i)T_0\\&+\frac{\chi}{2}(h_o-h_i)T_1+\frac{\chi h}{4}(h_o+h_i)T_2-\frac{\chi}{h}(h_o\Theta_o+h_i\Theta_i)-\frac{\chi Q_0}{\lambda_0 h}=0\\&\frac{\partial}{\partial t}(T_1)-\frac{\chi}{a^2}\Big[\gamma\frac{\partial}{\partial\xi}(T_1)+\frac{\partial^2}{\partial\xi^2}(T_1)+\frac{1}{\rho^2}\frac{\partial^2}{\partial\theta^2}(T_1)\Big]+\frac{6\chi}{h^2}(h_o-h_i)T_0+\frac{3\chi}{h}\Big(h_o+h_i+\frac{4}{h}\Big)T_1\\&+\frac{3\chi}{2}(h_o-h_i)T_2-\frac{6\chi}{h^2}(h_o\Theta_o-h_i\Theta_i)-\frac{12\chi Q_1}{\lambda_0 h^3}=0\\&\frac{\partial}{\partial t}(T_0)+\frac{3h^2}{20}\frac{\partial}{\partial t}(T_2)-\frac{\chi}{a^2}\Big[\gamma\frac{\partial}{\partial\xi}(T_0)+\frac{\partial^2}{\partial\xi^2}(T_0)+\frac{1}{\rho^2}\frac{\partial^2}{\partial\theta^2}(T_0)+\frac{3h^2}{20}\Big\{\gamma\frac{\partial}{\partial\xi}(T_2)+\frac{\partial^2}{\partial\xi^2}(T_2)+\frac{1}{\rho^2}\frac{\partial^2}{\partial\theta^2}(T_2)\Big\}\Big]+\frac{3\chi}{h}(h_o+h_i)T_0\\&+\frac{3\chi}{2}(h_o-h_i)T_1+\frac{3\chi h}{4}(h_o+h_i)T_2-\frac{3\chi}{h}(h_o\Theta_o+h_i\Theta_i)-\frac{12\chi Q_2}{\lambda_0 h^3}=0\end{aligned}\right\}\quad(5)$$

where the boundary conditions given by Eqs. (3) are substituted into the terms $[\partial T/\partial\zeta]_{-h/2}^{h/2}$ which appear in the integrations. In Eqs. (5) Q_0, Q_1 and Q_2 are given by

$$Q_n=\int_{-h/2}^{h/2}\eta_0\zeta^n d\zeta\quad(n=0,1,2).\quad(6)$$

For three independent variables T_0, T_1 and T_2, Eqs. (5) are given, and by solving these equations, the temperature field in the shell can be determined.

In recent years another analytical method for the heat conduction problem of axisymmetrical shells was proposed by Updike and Kalnins[15].

2.2 Thermal deformation equations

Eliminating the transverse shear forces Q_ξ and Q_θ in the equilibrium equations in the Sanders theory[13], and expressing in the rate forms, the following equations are obtained.

$$\left.\begin{aligned}&a\Big[\frac{\partial}{\partial\xi}(\rho\dot N_\xi)+\frac{\partial}{\partial\theta}(\dot N_{\xi\theta})-\rho'\dot N_\theta\Big]+\omega_\xi\Big[\frac{\partial}{\partial\xi}(\rho\dot M_\xi)+\frac{\partial}{\partial\theta}(\dot M_{\xi\theta})-\rho'\dot M_\theta\Big]+\frac{1}{2}(\omega_\xi-\omega_\theta)\frac{\partial}{\partial\theta}(\dot M_{\xi\theta})+\rho a^2\dot P_\xi=0\\&a\Big[\frac{\partial}{\partial\theta}(\dot N_\theta)+\frac{\partial}{\partial\xi}(\rho\dot N_{\xi\theta})+\rho'\dot N_{\xi\theta}\Big]+\omega_\theta\Big[\frac{\partial}{\partial\theta}(\dot M_\theta)+\frac{\partial}{\partial\xi}(\rho\dot M_{\xi\theta})+\rho'\dot M_{\xi\theta}\Big]+\frac{1}{2}\rho\frac{\partial}{\partial\xi}[(\omega_\theta-\omega_\xi)\dot M_{\xi\theta}]+\rho a^2\dot P_\theta=0\end{aligned}\right\}\quad(7)$$

$$\left.\begin{aligned}&\frac{\partial}{\partial\xi}\left[\frac{\partial}{\partial\xi}(\rho\dot{M}_\xi)+\frac{\partial}{\partial\theta}(\dot{\bar{M}}_{\xi\theta})-\rho'\dot{M}_\theta\right]\\&+\frac{1}{\rho}\frac{\partial}{\partial\theta}\left[\frac{\partial}{\partial\theta}(\dot{M}_\theta)+\frac{\partial}{\partial\xi}(\rho\dot{\bar{M}}_{\xi\theta})+\rho'\dot{\bar{M}}_{\xi\theta}\right]\\&-\alpha\rho(\omega_\xi\dot{N}_\xi+\omega_\theta\dot{N}_\theta)+\rho a^2\dot{P}_\zeta=0\end{aligned}\right\}$$

where $\bar{N}_{\xi\theta}$ and $\bar{M}_{\xi\theta}$ are the modified stress resultant and modified stress couple, respectively, and are expressed as follows[13]:

$$\left.\begin{aligned}\dot{\bar{N}}_{\xi\theta}&=(\dot{N}_{\xi\theta}+\dot{N}_{\theta\xi})/2\\&+[(1/R_\theta)-(1/R_S)](\dot{M}_{\xi\theta}-\dot{M}_{\theta\xi})/4\\\dot{\bar{M}}_{\xi\theta}&=(\dot{M}_{\xi\theta}+\dot{M}_{\theta\xi})/2\end{aligned}\right\}. \quad (8)$$

The other notations are shown in Fig. 1.

On the boundary, the effective membrane force $\hat{N}_{\xi\theta}$ and the effective transverse shear force $\hat{Q}_\xi$ per unit length are defined as follows[13]:

$$\left.\begin{aligned}\dot{\hat{N}}_{\xi\theta}&=\dot{\bar{N}}_{\xi\theta}+\frac{1}{2}\left(\frac{3}{R_\theta}-\frac{1}{R_S}\right)\dot{\bar{M}}_{\xi\theta}\\\dot{\hat{Q}}&=\frac{1}{a\rho}\left[\frac{\partial}{\partial\xi}(\rho\dot{M}_\xi)+2\frac{\partial}{\partial\theta}(\dot{\bar{M}}_{\xi\theta})-\rho'\dot{M}_\theta\right]\end{aligned}\right\}. \quad (9)$$

The strain rates of the middle surface are given by[13]:

$$\left.\begin{aligned}\dot{\varepsilon}_{\xi m}&=\frac{1}{a}\left[\frac{\partial}{\partial\xi}(\dot{U}_\xi)+\omega_\xi\dot{W}\right]\\\dot{\varepsilon}_{\theta m}&=\frac{1}{a}\left[\frac{1}{\rho}\frac{\partial}{\partial\theta}(\dot{U}_\theta)+\gamma\dot{U}_\xi+\omega_\theta\dot{W}\right]\\\dot{\varepsilon}_{\xi\theta m}&=\frac{1}{2a}\left[\frac{1}{\rho}\frac{\partial}{\partial\theta}(\dot{U}_\xi)+\frac{\partial}{\partial\xi}(\dot{U}_\theta)-\gamma\dot{U}_\theta\right]\end{aligned}\right\} \quad (10)$$

where $\dot{\varepsilon}_{\xi\theta m}$ is half the usual engineering shear strain rate. The bending distortion rates $\dot{\varkappa}_\xi$, $\dot{\varkappa}_\theta$ and $\dot{\varkappa}_{\xi\theta}$ are as follows:

$$\left.\begin{aligned}\dot{\varkappa}_\xi&=\frac{1}{a}\frac{\partial}{\partial\xi}(\dot{\Phi}_\xi),\quad \dot{\varkappa}_\theta=\frac{1}{a}\left\{\frac{1}{\rho}\frac{\partial}{\partial\theta}(\dot{\Phi}_\theta)+\gamma\dot{\Phi}_\xi\right\}\\\dot{\varkappa}_{\xi\theta}&=\frac{1}{2a}\left[\frac{1}{\rho}\frac{\partial}{\partial\theta}(\dot{\Phi}_\xi)+\frac{\partial}{\partial\xi}(\dot{\Phi}_\theta)-\gamma\dot{\Phi}_\theta\right.\\&\left.+\frac{1}{2a}(\omega_\xi-\omega_\theta)\left\{\frac{1}{\rho}\frac{\partial}{\partial\theta}(\dot{U}_\xi)-\frac{\partial}{\partial\xi}(\dot{U}_\theta)-\gamma\dot{U}_\theta\right\}\right]\end{aligned}\right\} \quad (11)$$

where rotation rates $\dot{\Phi}_\xi$ and $\dot{\Phi}_\theta$ are:

$$\left.\begin{aligned}\dot{\Phi}_\xi&=\frac{1}{a}\left[-\frac{\partial}{\partial\xi}(\dot{W})+\omega_\xi\dot{U}_\xi\right]\\\dot{\Phi}_\theta&=\frac{1}{a}\left[-\frac{1}{\rho}\frac{\partial}{\partial\theta}(\dot{W})+\omega_\theta\dot{U}_\theta\right]\end{aligned}\right\}. \quad (12)$$

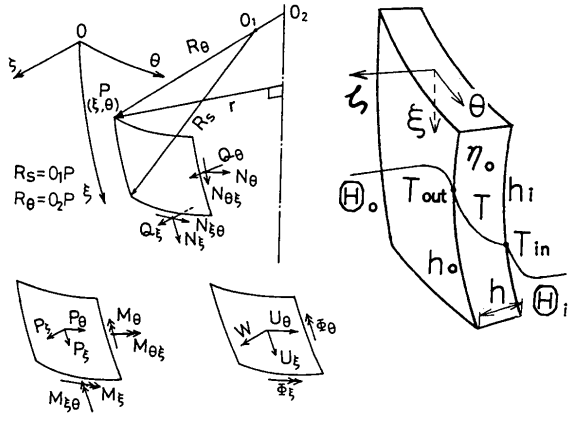

Fig. 1 Coordinates and notations

Under the Kirchhoff-Love hypothesis and the neglect of quantities ζ/R_S and ζ/R_θ which are small in comparison with unity, the strain rates at the distance ζ from the middle surface are

$$\{\dot{\varepsilon}\}=\{\dot{\varepsilon}_m\}+\zeta\{\dot{\varkappa}\} \quad (13)$$

where

$$\left.\begin{aligned}\{\dot{\varepsilon}\}&=\{\dot{\varepsilon}_\xi,\ \dot{\varepsilon}_\theta,\ \dot{\varepsilon}_{\xi\theta}\}^T\\\{\dot{\varepsilon}_m\}&=\{\dot{\varepsilon}_{\xi m},\ \dot{\varepsilon}_{\theta m},\ \dot{\varepsilon}_{\xi\theta m}\}^T\\\{\dot{\varkappa}\}&=\{\dot{\varkappa}_\xi,\ \dot{\varkappa}_\theta,\ \dot{\varkappa}_{\xi\theta}\}^T\end{aligned}\right\} \quad (14)$$

and $\{\ \}^T$ represents the transposed matrix.

Now we use the elasto/visco-plastic equations by Perzyna[14] considering the temperature effect for constitutive relations. The visco-plastic strain rates $\dot{\varepsilon}_{ij}^{vp}$ are

$$\dot{\varepsilon}_{ij}^{vp}=\gamma_0(T)\langle\Psi(f)\rangle S_{ij}J_2^{-1/2} \quad (15)$$

where the dot denotes partial differentiation with respect to time; S_{ij}, J_2 and $\gamma_0(T)$ are the deviatoric stress, the second invariant of the deviatoric stress tensor and a material constant, respectively, and γ_0 is a function of absolute temperature T as well as σ^* in Eq. (17). The symbol $\langle\Psi(f)\rangle$ is defined by:

$$\langle\Psi(f)\rangle=0:\ f\leqq 0\quad \langle\Psi(f)\rangle=\Psi(f):\ f>0 \quad (16)$$

where

$$f=\{\bar{\sigma}-\sigma^*(T)\}/\sigma^*(T) \quad (17)$$

and $f=0$ denotes the von Mises yield surface, $\bar{\sigma}$ is the equivalent stress $(=\sqrt{3J_2})$ and $\sigma^*(T)$ is the static stress determined from the elasto-plastic stress-strain relation in a usual tension test.

In the present paper, when we assume that the total strain rate may be composed of the elastic, the visco-plastic and the thermal parts, the total strain rates in the plane stress state are written as

$$\{\dot{\varepsilon}\}=[D]^{-1}\{\dot{\sigma}\}+\{\dot{\varepsilon}^{vp}\}+\{\dot{\varepsilon}^t\} \quad (18)$$

where

$$\left.\begin{aligned}\{\dot{\sigma}\}&=\{\dot{\sigma}_\xi,\ \dot{\sigma}_\theta,\ \dot{\sigma}_{\xi\theta}\}^T\\\{\dot{\varepsilon}^{vp}\}&=\{\dot{\varepsilon}_\xi^{vp},\ \dot{\varepsilon}_\theta^{vp},\ \dot{\varepsilon}_{\xi\theta}^{vp}\}^T\\\{\dot{\varepsilon}^t\}&=\{\alpha\dot{T}_e,\ \alpha\dot{T}_e,\ 0\}^T\\[D]&=\frac{E}{1-\nu^2}\begin{bmatrix}1&\nu&0\\\nu&1&0\\0&0&1-\nu\end{bmatrix}\\\{\dot{\varepsilon}^{vp}\}&=\frac{2}{\sqrt{3}}\gamma_0(T)\left\langle\Psi\left(\frac{\bar{\sigma}-\sigma^*(T)}{\sigma^*(T)}\right)\right\rangle\\&\times\frac{1}{\bar{\sigma}}\begin{bmatrix}1&-1/2&0\\-1/2&1&0\\0&0&3/2\end{bmatrix}\{\sigma\}\end{aligned}\right\}. \quad (19)$$

E, ν and α are Young's modulus, Poisson's ratio, and thermal expansion coefficient, and T_e is the temperature rise from the original temperature $\bar{T}_0$ to the present temperature T, namely,

$$T_e(\xi,\theta,\zeta,t)=T(\xi,\theta,\zeta,t)-\bar{T}_0. \quad (20)$$

Substituting Eqs. (13) into Eqs. (18) and solving them for stresses, we obtain

$$\{\dot{\sigma}\}=[D](\{\dot{\varepsilon}_m\}+\zeta\{\dot{\varkappa}\})-\{\dot{\sigma}^{vp}\}-\{\dot{\sigma}^t\} \quad (21)$$

where

$$\left.\begin{aligned}&\{\dot{\sigma}^{vp}\}=\{\dot{\sigma}_\xi^{vp},\ \dot{\sigma}_\theta^{vp},\ \dot{\sigma}_{\xi\theta}^{vp}\}^T=[D]\{\dot{\varepsilon}^{vp}\}\\&\{\dot{\sigma}^t\}=\{\dot{\sigma}^t,\ \dot{\sigma}^t,\ 0\}^T=[D]\{\dot{\varepsilon}^t\}\\&\quad=\frac{\alpha E}{1-\nu}\{\dot{T}_e,\ \dot{T}_e,\ 0\}^T\end{aligned}\right\}. \tag{22}$$

The membrane forces and the resultant moments per unit length are obtained from Eqs. (21) :

$$\left.\begin{aligned}&\{\dot{N}\}=\{\dot{N}_\xi,\ \dot{N}_\theta,\ \dot{N}_{\xi\theta}\}^T\\&\quad=h[D]\{\dot{\varepsilon}_m\}-\{\dot{N}^{vp}\}-\{\dot{N}^t\}\\&\{\dot{M}\}=\{\dot{M}_\xi,\ \dot{M}_\theta,\ \dot{M}_{\xi\theta}\}^T\\&\quad=\frac{h^3}{12}[D]\{\dot{\varkappa}\}-\{\dot{M}^{vp}\}-\{\dot{M}^t\}\end{aligned}\right\}. \tag{23}$$

In Eqs. (23), $(\ )^{vp}$ and $(\ )^t$ denote the apparent internal forces due to visco-plasticity and the internal forces due to temperature rise T_e, respectively, and are given by :

$$\left.\begin{aligned}&\{\dot{N}^{vp},\ \dot{N}^t\}=\int_{-h/2}^{h/2}\{\dot{\sigma}^{vp},\ \dot{\sigma}^t\}d\zeta\\&\{\dot{M}^{vp},\ \dot{M}^t\}=\int_{-h/2}^{h/2}\{\dot{\sigma}^{vp},\ \dot{\sigma}^t\}\zeta d\zeta\end{aligned}\right\}. \tag{24}$$

A complete set of field equations for the 36 independent variables $\{\dot{N}\}$, $\{\dot{M}\}$, $\{\dot{N}^{vp}\}$, $\{\dot{M}^{vp}\}$, $\{\dot{N}^t\}$, $\{\dot{M}^t\}$, $\{\dot{\sigma}\}$, $\{\dot{\sigma}^{vp}\}$, $\{\dot{\sigma}^t\}$, $\{\dot{\varepsilon}_m\}$, $\{\dot{\varepsilon}^{vp}\}$, $\{\dot{\varepsilon}^t\}$, $\dot{U}_\xi$, $\dot{U}_\theta$, $\dot{W}$, $\{\dot{\varkappa}\}$, $\dot{\Phi}_\xi$ and $\dot{\Phi}_\theta$ is now given by the 36 equations (7), (10)～(12), (19) and (21)～(24).

3. Nondimensional Equations

In order to analyze the problem of shells under arbitrary unsymmetrical loads, the distributed loads, the ambient fluid temperature, the heat generation and the 35 independent variables mentioned in section 2, except for $\{\dot{\varepsilon}^{vp}\}$ and $\dot{\varepsilon}^t$, are expanded into the Fourier series as follows.

$$\left.\begin{aligned}&\{\dot{N}_\xi,\ \dot{N}_\xi^{vp},\ \dot{N}_\theta,\ \dot{N}_\theta^{vp},\ \dot{N}^t\}\\&\quad=\sigma_0 h\sum_{n=0}^{\infty}\{\dot{n}_\xi^{(n)},\ \dot{n}_\xi^{vp(n)},\ \dot{n}_\theta^{(n)}\dot{n}_\theta^{vp(n)},\ \dot{n}^{t(n)}\}\cos n\theta\\&\{\dot{M}_\xi,\ \dot{M}_\xi^{vp},\ \dot{M}_\theta,\ \dot{M}_\theta^{vp}\dot{M}^t\}\\&\quad=\frac{\sigma_0 h^3}{a}\sum_{n=0}^{\infty}\{\dot{m}_\xi^{(n)},\ \dot{m}_\xi^{vp(n)},\ \dot{m}_\theta^{(n)},\ \dot{m}_\theta^{vp(n)},\ \dot{m}^{t(n)}\}\cos n\theta\\&\{\dot{\bar{N}}_{\xi\theta},\ \dot{\bar{N}}_{\xi\theta}^{vp}\}=\sigma_0 h\sum_{n=1}^{\infty}\{\dot{\bar{n}}_{\xi\theta}^{(n)},\ \dot{\bar{n}}_{\xi\theta}^{vp(n)}\}\sin n\theta\\&\{\dot{\bar{M}}_{\xi\theta},\ \dot{\bar{M}}_{\xi\theta}^{vp}\}=\frac{\sigma_0 h^3}{a}\sum_{n=1}^{\infty}\{\dot{\bar{m}}_{\xi\theta}^{(n)},\ \dot{\bar{m}}_{\xi\theta}^{vp(n)}\}\sin n\theta\\&\{\dot{U}_\xi,\ \dot{W},\ \dot{\varepsilon}_{\xi m},\ \dot{\varepsilon}_{\theta m},\ \dot{\varkappa}_\xi,\ \dot{\varkappa}_\theta,\ \dot{\Phi}_\xi\}\\&\quad=\frac{\sigma_0}{E}\sum_{n=0}^{\infty}\left\{a\dot{u}_\xi^{(n)},\ a\dot{w}^{(n)},\ \dot{e}_{\xi m}^{(n)},\ \dot{e}_{\theta m}^{(n)},\ \frac{\dot{k}_\xi^{(n)}}{a},\ \frac{\dot{k}_\theta^{(n)}}{a},\right.\\&\quad\left.\dot{\varphi}_\xi^{(n)}\right\}\cos n\theta\\&\{\dot{U}_\theta,\ \dot{\varepsilon}_{\xi\theta m},\ \dot{\varkappa}_{\xi\theta},\ \dot{\Phi}_\theta\}\\&\quad=\frac{\sigma_0}{E}\sum_{n=1}^{\infty}\left\{a\dot{u}_\theta^{(n)},\ \dot{e}_{\xi\theta m}^{(n)},\ \frac{\dot{k}_{\xi\theta}^{(n)}}{a},\ \dot{\varphi}_\theta^{(n)}\right\}\sin n\theta\\&\{\dot{\sigma}_\xi,\ \dot{\sigma}_\xi^{vp},\ \dot{\sigma}_\theta,\ \dot{\sigma}_\theta^{vp},\ \dot{\sigma}^t,\ \dot{P}_\xi,\ \dot{P}_\zeta,\ T_0,\ T_1,\ T_2,\ \Theta_i,\ \Theta_o\}\\&\quad=\sigma_0\sum_{n=0}^{\infty}\left\{\dot{s}_\xi^{(n)},\ \dot{s}_\xi^{vp(n)},\ \dot{s}_\theta^{(n)},\ \dot{s}_\theta^{vp(n)},\ \dot{s}^{t(n)},\ \frac{h}{a}\dot{p}_\xi^{(n)},\right.\\&\left.\frac{h}{a}\dot{p}_\zeta^{(n)},\ \frac{t_0^{(n)}}{E\alpha},\ \frac{t_1^{(n)}}{Eah},\ \frac{t_2^{(n)}}{Eah^2},\ \frac{\theta_i^{(n)}}{E\alpha},\ \frac{\theta_0^{(n)}}{E\alpha}\right\}\cos n\theta\\&\{\dot{\sigma}_{\xi\theta},\ \dot{\sigma}_{\xi\theta}^{vp},\ \dot{p}_\theta\}\\&\quad=\sigma_0\sum_{n=1}^{\infty}\left\{\dot{s}_{\xi\theta}^{(n)},\ \dot{s}_{\xi\theta}^{vp(n)},\ \frac{h}{a}\dot{p}_\theta^{(n)}\right\}\sin n\theta\\&\{Q_0,\ Q_1,\ Q_2\}\\&\quad=\frac{\lambda_0}{a}\frac{\sigma_0}{E\alpha}\sum_{n=0}^{\infty}\{q_0^{(n)},\ hq_1^{(n)},\ h^2q_2^{(n)}\}\cos n\theta\end{aligned}\right\} \tag{25}$$

where σ_0 is a reference stress.

It should be noted that the Fourier expansions, Eqs. (25), are not the most general that could exist. For full generality, these expansions should be augmented by the sine-additional series for the cosine series and by the cosine-additional series for the sine series.

Substituting these into the above fundamental equations, the equations among the Fourier coefficients relating to the variables are obtained. From the heat conduction equations, the simultaneous differential equations for the coefficients $t_0^{(n)}$, $t_1^{(n)}$, $t_2^{(n)}$ can be obtained as

$$A_1Y''+A_2Y'+A_3Y=A_4+A_5(\partial Y/\partial\tau) \tag{26}$$

where $Y=\{t_0^{(n)},\ t_1^{(n)},\ t_2^{(n)}\}^T$ and $\tau=\chi t/a^2$. A_1～A_3 are 3×3 matrices determined from h_i, h_o and the shell form. A_4 is a 3×1 matrix determined from Θ_i, Θ_o, h_i and h_o. A_5 is a 3×3 constant matrix.

Similarly eliminating the variables from the thermal deformation equations, the simultaneous differential equations for the displacement rates $\dot{u}_\xi^{(n)}$, $\dot{u}_\theta^{(n)}$, $\dot{w}^{(n)}$ and the bending moment rate $\dot{m}_\xi^{(n)}$ can be derived as

$$B_1Z''+B_2Z'+B_3Z=B_4 \tag{27}$$

where $Z=\{\dot{u}_\xi^{(n)},\ \dot{u}_\theta^{(n)},\ \dot{w}^{(n)},\ \dot{m}_\xi^{(n)}\}$. B_1～B_3 are 4×4 matrices determined from the shell form and ν. B_4 is a 4×1 matrix determined from the distributed loads and the internal forces due to visco-plasticity and temperature rise in addition to the shell geometries[9].

On eliminating the strains and the bending distortions from Eqs. (21) and (23), and expressing these by the Fourier coefficients, the stresses are calculated from the following equations :

$$\left.\begin{aligned}\dot{s}_\xi&=\dot{n}_\xi+\dot{n}_\xi^{vp}+\dot{n}^t+12\frac{\zeta}{a}(\dot{m}_\xi+\dot{m}_\xi^{vp}+\dot{m}^t)\\&\quad-\dot{s}_\xi^{vp}-\dot{s}^t\\\dot{s}_\theta&=\dot{n}_\theta+\dot{n}_\theta^{vp}+\dot{n}^t+12\frac{\zeta}{a}(\dot{m}_\theta+\dot{m}_\theta^{vp}+\dot{m}^t)\\&\quad-\dot{s}_\theta^{vp}-\dot{s}^t\\\dot{s}_{\xi\theta}&=\dot{\bar{n}}_{\xi\theta}+\dot{\bar{n}}_{\xi\theta}^{vp}+12\frac{\zeta}{a}(\dot{\bar{m}}_{\xi\theta}+\dot{\bar{m}}_{\xi\theta}^{vp})-\dot{s}_{\xi\theta}^{vp}\end{aligned}\right\}. \tag{28}$$

The rates of internal forces related to the visco-plasticity and the temperature rise in Eqs. (27) and (28) become the following, by use of Eqs. (22), (24) and (25).

$$\left.\begin{aligned}
&\sigma_0 h\sum_{n=0}^{\infty}\{\dot{n}_\xi^{vp(n)},\ \dot{n}_\theta^{vp(n)},\ \dot{n}_{\xi\theta}^{vp(n)}\}[A_n]\\
&\quad=\int_{-h/2}^{h/2}\{\dot{\varepsilon}_\xi^{vp},\ \dot{\varepsilon}_\theta^{vp},\ \dot{\varepsilon}_{\xi\theta}^{vp}\}[D]d\zeta\\
&\frac{\sigma_0 h^3}{a}\sum_{n=0}^{\infty}\{\dot{m}_\xi^{vp(n)},\ \dot{m}_\theta^{vp(n)},\ \dot{m}_{\xi\theta}^{vp(n)}\}[A_n]\\
&\quad=\int_{-h/2}^{h/2}\{\dot{\varepsilon}_\xi^{vp},\ \dot{\varepsilon}_\theta^{vp},\ \dot{\varepsilon}_{\xi\theta}^{vp}\}[D]\zeta d\zeta\\
&\{\dot{n}^{t(n)},\ \dot{m}^{t(n)}\}=\frac{1}{h}\frac{1}{1-\nu}\int_{-h/2}^{h/2}\left\{1,\frac{a\zeta}{h^2}\right\}\dot{t}_e d\zeta
\end{aligned}\right\}\quad(29)$$

$$\sigma_0\sum_{n=0}^{\infty}\{\dot{s}_\xi^{vp(n)},\ \dot{s}_\theta^{vp(n)},\ \dot{s}_{\xi\theta}^{vp(n)}\}[A_n]=\{\dot{\varepsilon}_\xi^{vp},\ \dot{\varepsilon}_\theta^{vp},\ \dot{\varepsilon}_{\xi\theta}^{vp}\}[D]\quad(30)$$

where $[A_n]=[\cos n\theta, \cos n\theta, \sin n\theta]$ (diagonal matrix). The visco-plastic strain rates on the right-hand sides of Eqs. (29) and (30) can be related to the stresses by Eqs. (19). The integrations are carried out numerically using Simpson's 1/3 rule.

4. Numerical Method

A finite difference method is employed for the solutions of the two second order simultaneous differential equations (26) and (27). The usual central difference formulas are used for every mesh point except the discontinuity points and the boundary points of the shell. For the discontinuity points and the boundary points, forward and backward difference equations are employed[3]. The derivatives with respect to time in Eq. (26) are treated by the Crank-Nicolson method. The solutions at any time are obtained by a summation of the incremental values due to the time increment.

5. Numerical Example

As a numerical example, a simply supported internally pressurized cylindrical shell of aluminum subjected to locally distributed thermal loading due to fluid is analyzed (Fig. 2). $\bar{T}_o$ and Θ_i are both 25°C, and the boundary conditions at both ends are assumed to be adiabatic. h_i and h_o on inner and outer surfaces of the shell are both 0.23/m, and internal pressure P_ζ is 0.

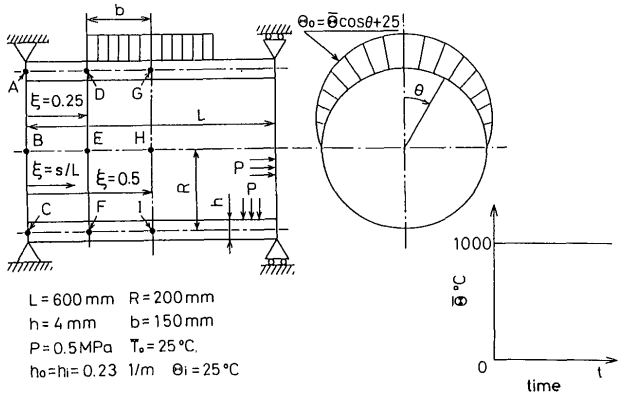

Fig. 2 Numerical example

5 MPa. The value of σ_0 in Eqs. (25) has been selected as $\sigma_0=1$.

The geometrical parameters of the shell are

$$\left.\begin{aligned}
&a=L,\ \xi=s/L,\ \rho=1/3,\ \rho'=0,\ \gamma=0\\
&\omega_\theta=3,\ \omega_\xi=\omega'_\xi=0
\end{aligned}\right\}\quad(31)$$

where L is length of the shell.

The meridional increment $\Delta\xi$ in the finite difference calculation is

$$\Delta\xi=1/\{2(N-1)\}\quad(32)$$

where N is the number of mesh points.

Boundary conditions relating to thermal deformation equations at the points A ($i=1$) and G ($i=N$) are

$$\left.\begin{aligned}
&\text{Point A: } \dot{U}_\theta=\dot{W}=\dot{M}_\xi=0,\ \dot{N}_\xi=\dot{P}_\zeta\cdot R/2\\
&\text{Point G: } \dot{U}_\xi=\dot{\bar{N}}_{\xi\theta}=\dot{\bar{Q}}_\xi=\dot{\Phi}_\xi=0
\end{aligned}\right\}.\quad(33)$$

The material constants employed in the calculations are as follows.

$$\left.\begin{aligned}
&E=69\text{ GPa},\ \rho_0=2.71\text{ g/cm}^3\\
&\nu=0.33,\ \lambda_0=222\text{ W/(m·K)}\\
&\alpha=23.6\times10^{-6}\text{ K}^{-1},\ c=0.904\text{ kJ/(kg·K)}\\
&\sigma^*(T)=-0.011(T/100)^4+0.22(T/100)^3\\
&\quad+0.6(T/100)^2-25.6(T/100)+92.6\text{ MPa}\\
&\gamma_0(T)=\exp\{-(T-302.5)/15.4\}\text{ s}^{-1}\\
&\Psi(f)=[(\bar{\sigma}-\sigma^*(T))/\sigma^*(T)]^{10}
\end{aligned}\right\}\quad(34)$$

where the unit of temperature T is degree centigrade. Using these material constants, the stress-strain curves of the material at $T=25$, 200, 300 and 400°C are obtained as shown in Fig. 3.

The number of mesh points N and the number of divisions through the thickness are chosen to be 101 and 19, respectively. The number of terms of the Fourier series is selected to be $n=20$, and the increment of time Δt is selected as 0.1 sec. These values are chosen with consideration of the convergence of the solutions, the capacity of the computer and computing time.

Now we shall discuss some results of calculation.

The variations of temperature distribution through the thickness at point G ($\xi=0.5$, $\theta=0°$) of the shell are shown in Fig. 4. In this figure the results from the present theory are plotted by solid lines, and

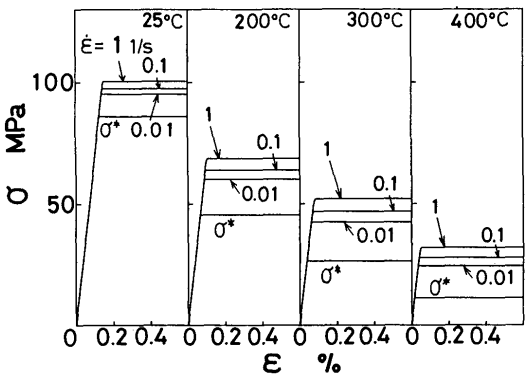

Fig. 3 Stress-strain relations

the results based on the assumption of linear temperature distribution through the thickness are plotted by broken lines. In this numerical example both results almost agree, and the distributions through the thickness become uniform after about $t=2$ sec. Therefore in the following figures we shall indicate the temperature on the middle surface of the shell.

Figure 5 illustrates the variations with time of temperature at points A~I ($\xi=0, 0.25, 0.5$: $\theta=0°$, 90°, 180°). Figure 6 gives the meridional distributions of the temperature along $\theta=0°, 90°, 180°$, and the circumferential distributions along $\xi=0, 0.25, 0.5$. In the heated region the temperature rises quickly in comparison with other areas, and subsequently increases gradually until the steady state is reached.

Figure 7 shows the variations with time of meridional displacement U_ξ at points A~C ($\xi=0$; $\theta=0°$, 90°, 180°), radial displacement W at points G~I ($\xi=0.5$; $\theta=0°, 90°, 180°$) and circumferential displacement U_θ at point H. In Figs. 8 and 9, the meridional distributions of displacements along $\theta=0°, 90°, 180°$, and the circumferential distributions along $\xi=0, 0.5$ are illustrated, respectively. Although about a quarter of the yielding internal pressure is applied, axisymmetrical deformations by the pressure are very small in comparison with thermal deformations, and only the distribution of W can be recognized in these figures. From Figs. 8 and 9, a large deformation occurs in the high temperature region where heating

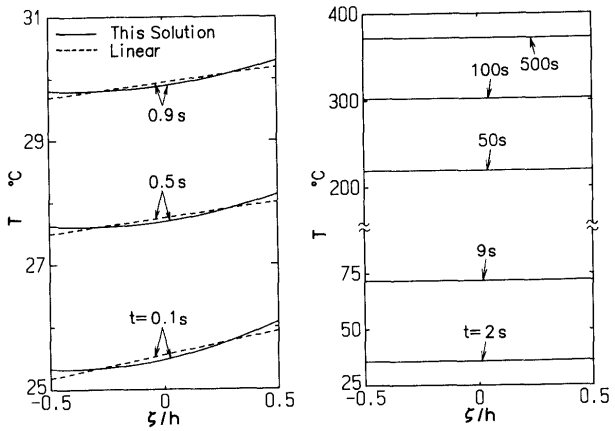

Fig. 4 Temperature distributions through thickness at point G ($\xi=0.5$, $\theta=0°$)

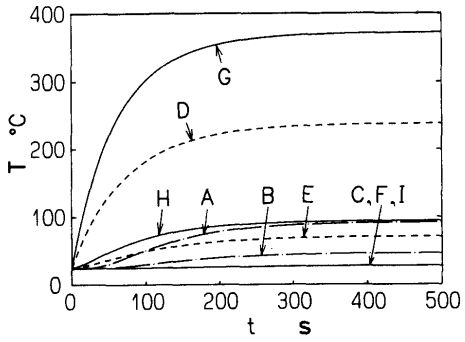

Fig. 5 Variations of temperature at specific points with time

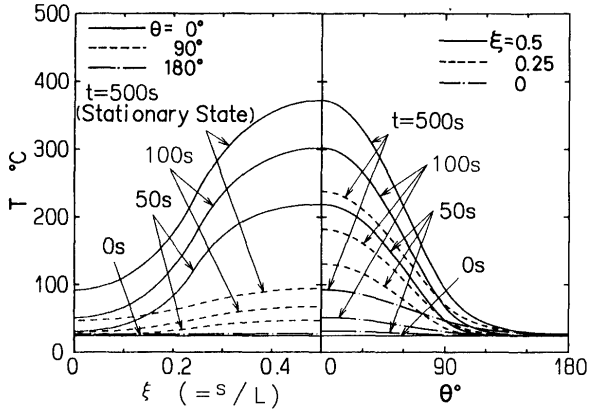

Fig. 6 Meridional and circumferential distributions of temperature with time

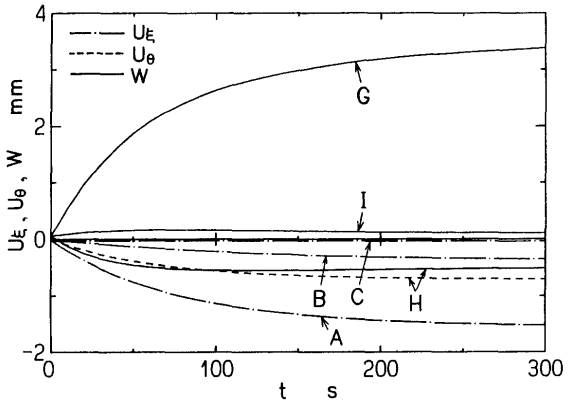

Fig. 7 Variations of displacements at specific points with time

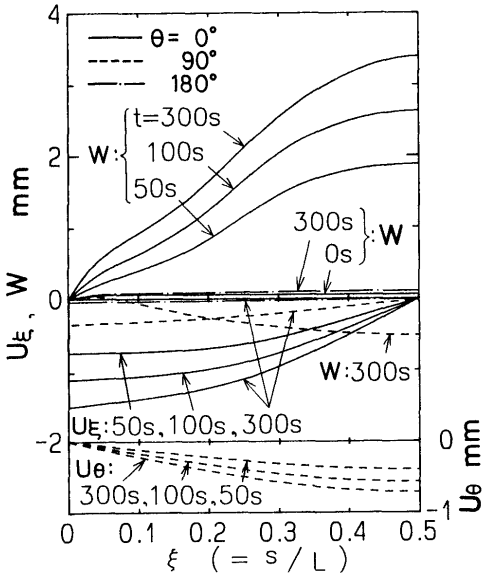

Fig. 8 Meridional distributions of displacements with time

load is directly applied. Under this influence, U_θ and W near $\theta=90°$ on the middle cross section and U_ξ near the supported edges have negative values.

Figure 10 shows the variations with time of resultant stress N_ξ at points G~I, resultant stress N_θ at points A~C, G~I and resultant stress $\bar{N}_{\xi\theta}$ at points B and E. Meridional and circumferential distributions of these resultant stresses are also depicted in Figs. 11 and 12, respectively. The value of N_ξ is initially 50 N/mm in tension throughout the shell body, and varies with heat loading until the steady state is reached at about 100 seconds. N_ξ varies monotonically with ξ, but circumferential distribution becomes nonuniform towards the middle part of the shell. The value of N_θ is initially about 100 N/mm in tension except near the edges ($\xi=0\sim0.06$). About 20 seconds later N_θ becomes locally large compression at $\theta=0°\sim90°$ near the edges due to heat conduction. After yielding occurs at $t=150$ sec, there are few changes in N_θ with time. Near point D, where the temperature gradient is large, slight meridional variation of N_θ appears. In these figures $\bar{N}_{\xi\theta}$ at $t=300$ sec is also plotted, but this value is small in comparison with N_ξ and N_θ.

Figure 13 shows the variations with time of resultant moments M_ξ, M_θ at points D~I and resultant moment $\bar{M}_{\xi\theta}$ at points B and E. Figures 14 and 15 represent the variations of distributions of resultant moments with time. M_ξ and M_θ show similar distributions and variations with time, but M_ξ is large near point A ($\xi\fallingdotseq0.03$). Both moments show meridional variation near point D, and decrease markedly near

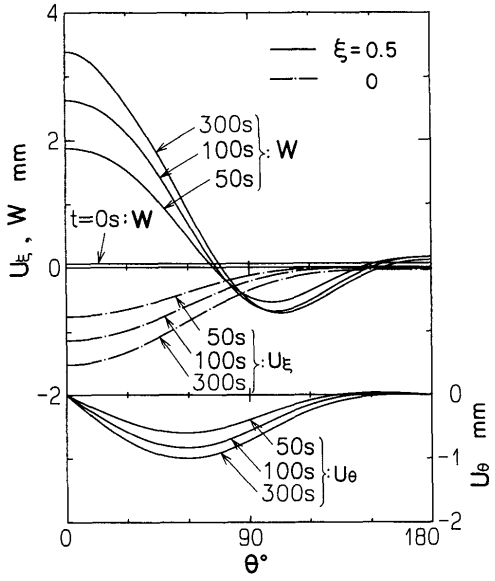

Fig. 9 Circumferential distributions of displacements with time

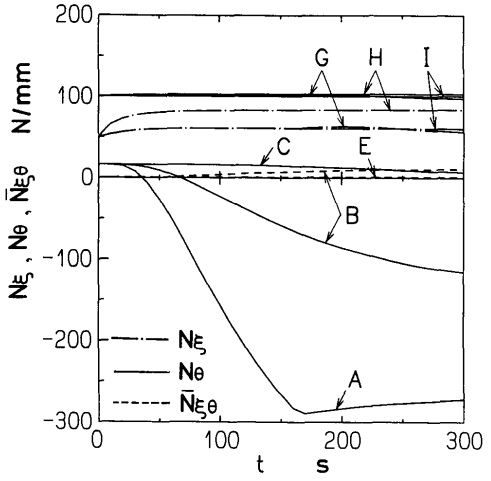

Fig. 10 Variations of resultant forces at specific points with time

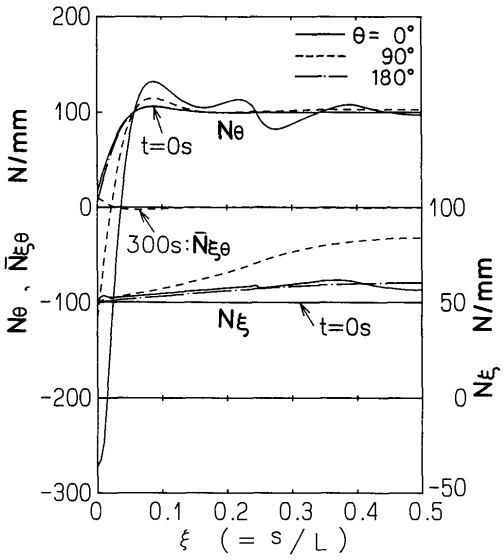

Fig. 11 Meridional distributions of resultant forces with time

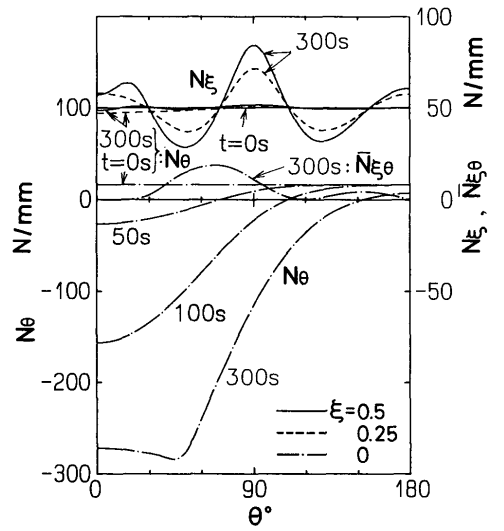

Fig. 12 Circumferential distributions of resultant forces with time

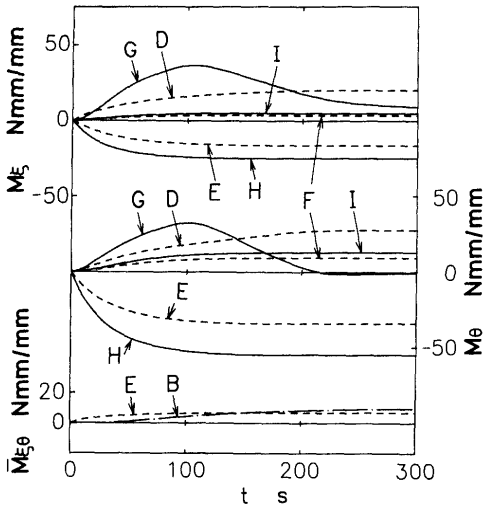

Fig. 13 Variations of resultant moments at specific points with time

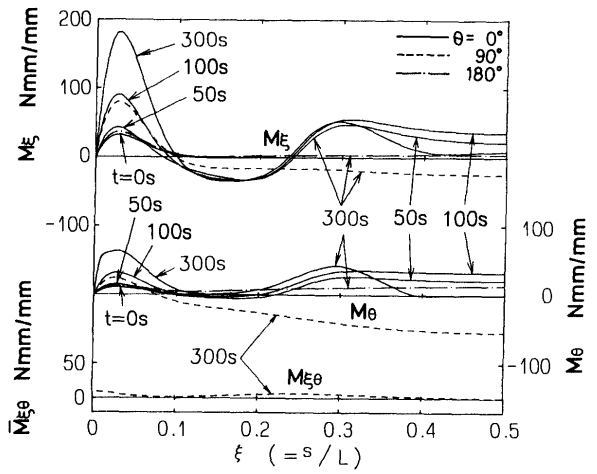

Fig. 14 Meridional distributions of resultant moments with time

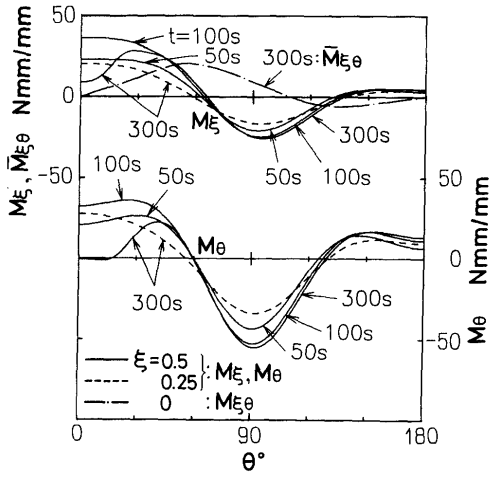

Fig. 15 Circumferential distributions of resultant moments with time

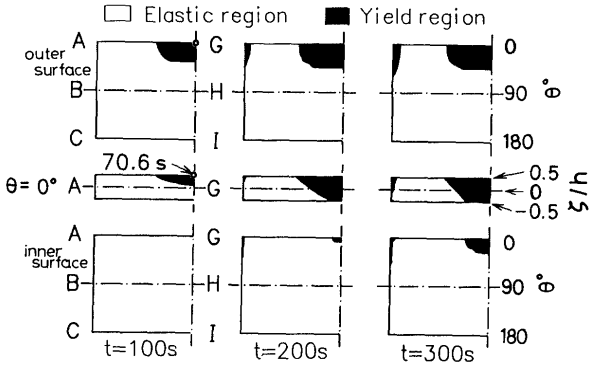

Fig. 16 Progressions of yield

point G with expansion of yield region. Resultant moment $\bar{M}_{\xi\theta}$ is large near $\theta=50°$ at the edges.

Figure 16 illustrates the aspect of the progression of yield. At about $t=70.6$ sec, yielding occurs on the outer surface at point G, and with the lapse of time the yield region expands in the thickness, meridional and circumferential directions. Yielding also occurs in the region of supported edges. The yielding zones on the outer surface of the shell are larger than those on the inner surface.

6. Conclusions

In this paper we have described the numerical analysis of the elasto/visco-plastic deformation of axisymmetrical thin shells subjected to thermal loads due to fluid. The temperature distribution through the thickness has been assumed to be a curve of the second order, and the equations of heat conduction and heat transfer have been solved under appropriate initial and boundary conditions.

By using the temperature distributions obtained, the stresses and deformations have been calculated from the thermal stress equations. The equations of equilibrium and the strain displacement relations have been derived from the Sanders thin shell theory. The constitutive equations by Perzyna, considering the temperature effect, have been employed. The numerical method selected for this problem is a method using finite difference in both space and time.

As a numerical example, the internally pressurized cylindrical shell subjected to locally distributed thermal loads due to fluid has been analyzed.

From the calculations, we found the following.

(1) Displacements and internal forces vary gradually with the temperature rise of the shell, and tend to the steady state.

(2) Spring back of displacements and relaxation of internal forces occur in the yield region.

(3) Resultant stress N_θ and resultant moments M_ξ, M_θ have large values on the edges of the shell and near the edges, respectively, and they show meridional variations near the boundary of the heated region.

References

(1) Nagarajan, S. and Popov, E.P., Plastic and Visco-plastic Analysis of Axisymmetric Shells, Int. J. Solids and Struct., Vol. 11(1975), p. 1.

(2) Kanchi, M.B., Zienkiewicz, O.C. and Owen, D.R.J., The Visco-Plastic Approach to Problems of Plasticity and Creep Involving Geometric Non-Linear Effects, Int. J. for Numerical Methods in Eng., Vol. 12(1978), p. 169.

(3) Tao, K. and Takezono, S., Elasto/Visco-Plastic Analysis of Axisymmetrical Shells under Asymmetrical Loading, Trans. 5th Int. Conf. Struct. Mech. in Reactor Technol., Vol. M(1979), M 4/8.

(4) Atkatsh, R.S., Bieniek, M.P. and Sandler, I.S., Theory of Visco-Plastic Shells for Dynamic Response, Trans. ASME, J. Appl. Mech., Vol. 50, No. 1(1983), p. 131.

(5) Tao, K. and Takezono, S., Analysis of Elasto/Visco-Plastic Dynamic Response of General Thin Shells by Means of Overlay Model, JSME Int. J., Ser. I, Vol. 33, No. 3(1990), p. 326.

(6) Takezono, S., Tao, K. and Tani, K., Elasto/Visco-Plastic Deformation of Multi-Layered Moderately Thick Shells of Revolution, JSME Int. J., Ser. I, Vol. 34, No. 1(1991), p. 13.

(7) Takezono, S., Tao, K. and Taguchi, T., Elasto/Visco-Plastic Dynamic Response of Multi-Layered Moderately Thick Shells of Revolution, Trans. 11th Int. Conf. Struct. Mech. in Reactor Technol., Vol. L(1991), p. 73.

(8) Wojewódzki, W. and Bukowski, R., Influence of the Yield Function Nonlinearity and Temperature in Dynamic Buckling of Viscoplastic Cylindrical Shells, Trans. ASME, J. Appl. Mech., Vol. 51, No. 1(1984), p. 114.

(9) Takezono, S. and Tao, K., Elasto/Visco-Plastic Dynamic Response of Thin Shells of Revolution Subjected to Mechanical or Thermal Loads or Both, Int. J. Pressure Vessels and Piping, Vol. 44(1990), p. 309.

(10) Bolotin, V.V., Equations for the Non-Stationary Temperature Fields in Thin Shells in the Presence of Sources of Heat, PMM, Vol. 24, No. 2(1960), p. 515.

(11) Shirakawa, K. and Ochiai, Y., Transient Response of Cylindrical Shells to Localized Heat Sources, Nucl. Eng. and Design, Vol. 54(1979), p. 337.

(12) Mizoguchi, K., On Thermoelasticity of Cylindrical Shells, Bull. Univ. Osaka Pref., Ser. A, No. 15(1966), p. 1.

(13) Sanders, J.L., Jr., An Improved First-Approximation Theory for Thin Shells, NASA Tech. Rep., R-24(1959), p. 1.

(14) Perzyna, P., Fundamental Problems in Viscoplasticity, Adv. in Appl. Mech., Vol. 9(1966), p. 243, Academic Press.

(15) Updike, D.P. and Kalnins, A., Heat Conduction in Shells of Revolution. Num. Methods for Thermal Problems, Vol. 5, No. 1(1987), p. 265.